Surface diffusion constants and supersaturations in SmBCO films prepared by pulsed laser deposition method at various deposition conditions

*Y. Ichino, N. Shimazaki, Y. Tsuchiya, Y. Yoshida (Nagoya Univ.)

Acknowledgements
This work was partly supported by a Grant-in-Aid for Scientific Research (23226014, 25289358, 15H04252, 15K14301, 15K14302 and 16H04512) and the ALCA project of the Japan Science and Technology Agency (JST).

Outline

1. Introduction

(1) Favorable orientation of $REBa_2Cu_3O_y$ films

(2) Self-organization of Ba-M-O (BMO, M=Zr, Sn, Hf, Nb etc.)

Objective

2. Experimental

3. Results and discussion

(1) Surface diffusion constant

(2) Supersaturation and preferential orientation

4. Summary

(1) Favorable orientation of REBCO films

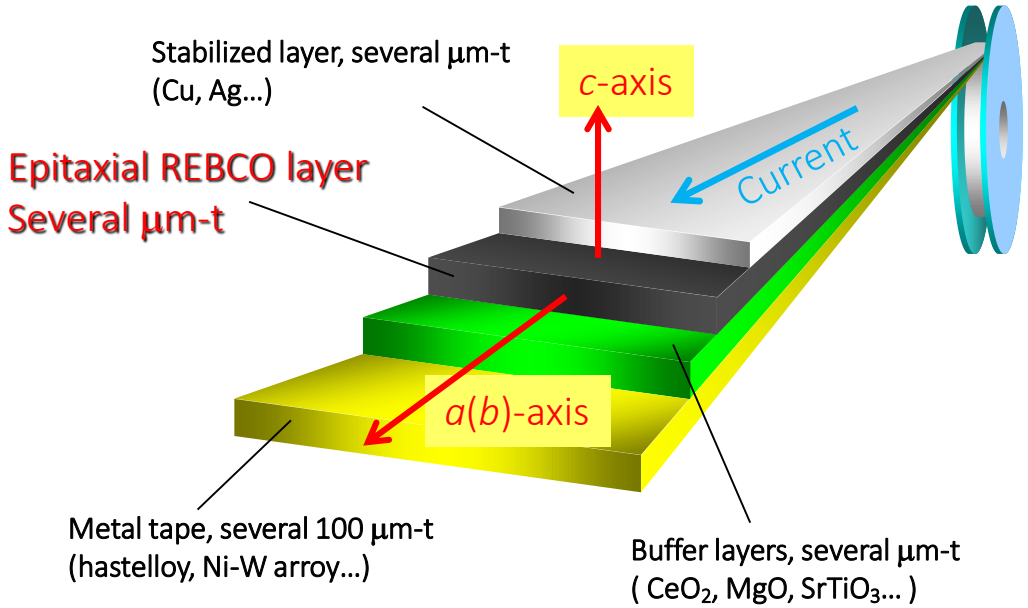

Fig. Schematic drawing of REBCO coated conductor.

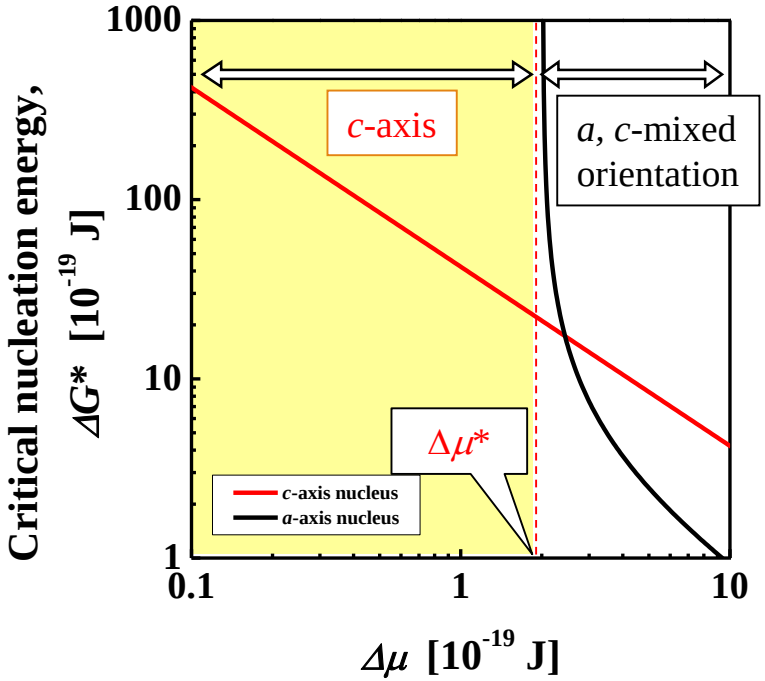

Fig. Critical nucleation energy of REBCO as a function of supersaturation.

ref. Y. Ichino et al., IEEE TAS 13 (2003) 2735

For large current carrying capability,

Favorable orientation → *c*-axis of REBCO ⊥ current

Previous study

Preferential orientation → **nucleation** in initial growth stage

c-axis nuclei → low supersaturation < $\Delta\mu^*$

(high substrate temperature, low growth rate…).

→ Supersaturation ($\Delta\mu$)

(2) Self-organization of Ba-M-O

In order to clarify self-organization mechanism of BMO → Monte Carlo simulation

Ref. Y. Ichino et al., **Jpn. J. Appl. Phys. 56 (2017) 015601**, IEEE TAS 27 (2017) 7500304

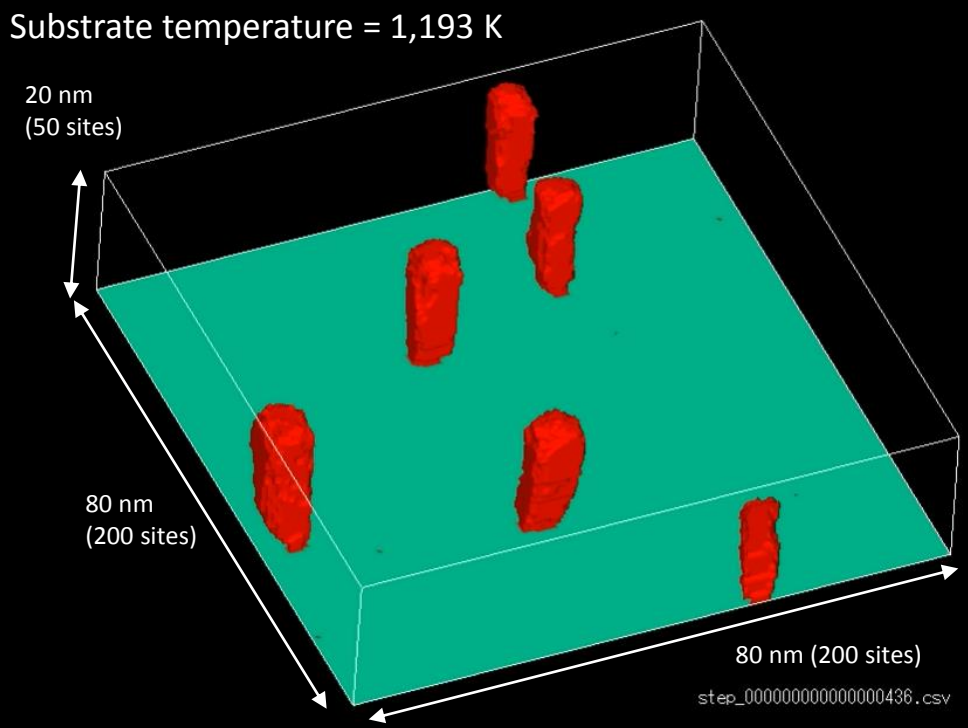

Fig. Bird's view of BMO self-organization. BMO particles were expressed by red cubes. REBCO particles were transparent for ease of viewing.

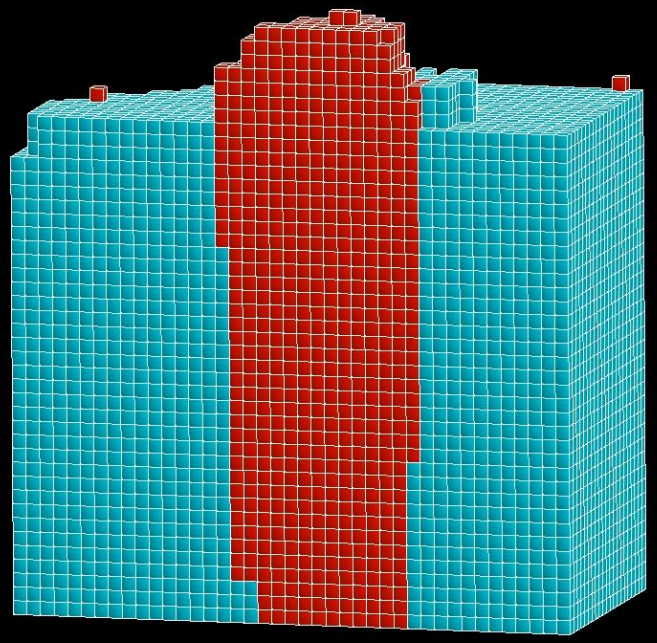

Fig. Magnified cross-sectional view of a nanorod in the left movie. Red cubes correspond to BMO and aqua blue ones are REBCO.

- BMO particles aggregated due to the unstable boundary between BMO and REBCO.
- BMO grew up 3D-island mode. REBCO was 2D-island growth mode.
- Top of the BMO is higher than the REBCO layer. → Consistent with experimental results

Substrate temp. dependence

Ref. Y. Ichino et al., Jpn. J. Appl. Phys. 56 (2017) 015601, IEEE TAS 27 (2017) 7500304

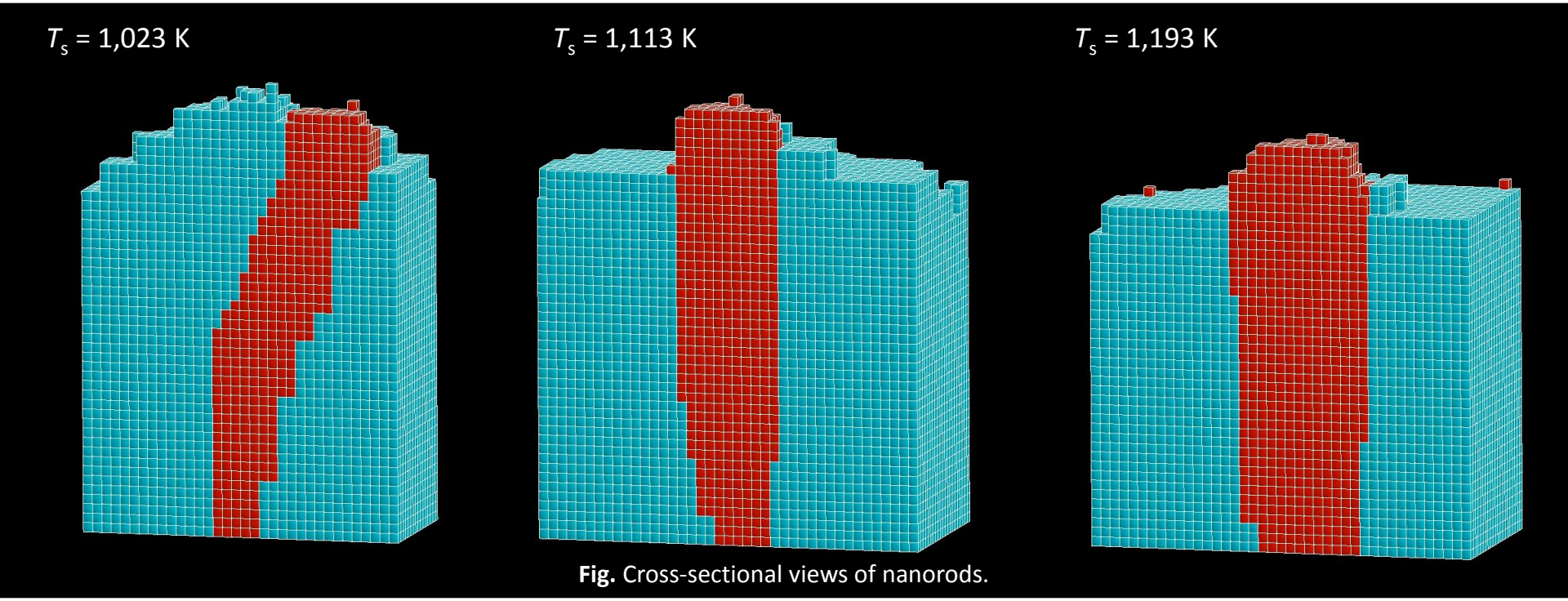

Fig. Cross-sectional views of nanorods.

- At T_s = 1,023 K, the nanorod tilted toward right, because the advance of the left side of the nanorod was restricted by the terrace of REBCO.

➔Inclined nanorods are observed in SmBCO films, experimentally.

ref. S. Miura et al., APL maters 4 (2016) 016102, T. Ozaki et al, J. Appl. Phys. 108 (2010) 093905

Phase diagram of Ba-M-O nanostructures

For suppression of flux motion → Control of BMO nanostructures

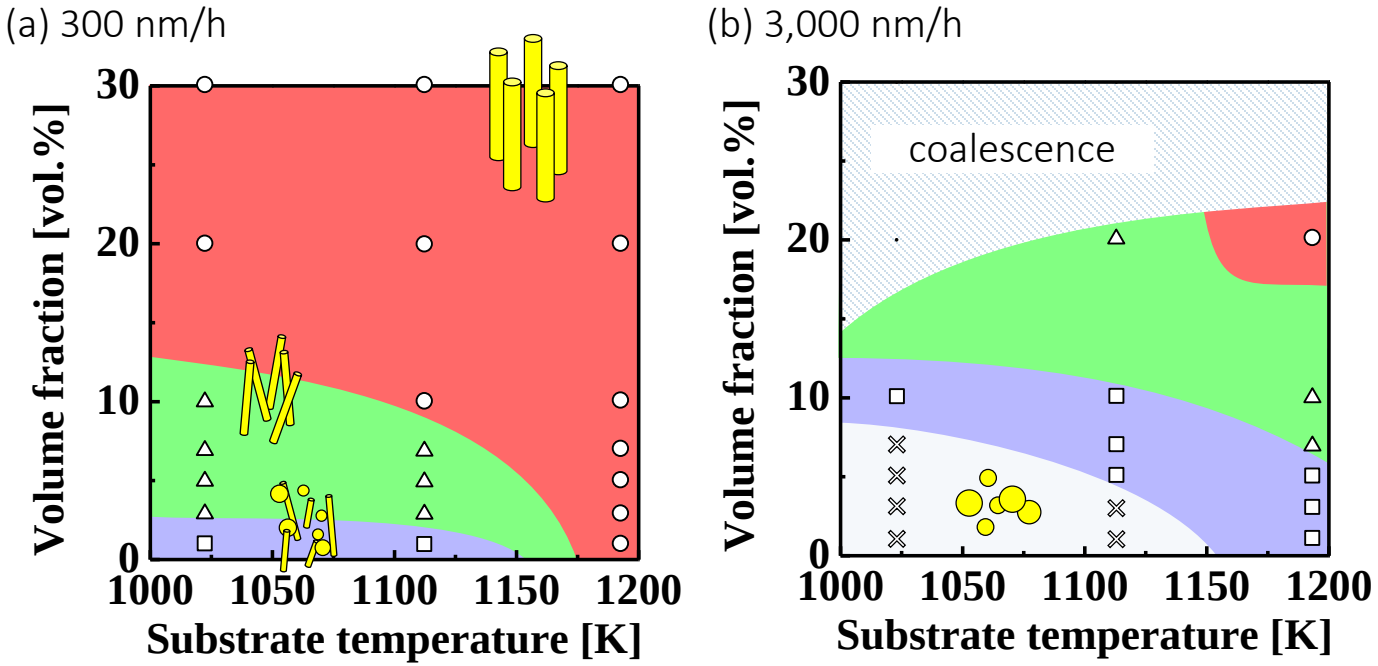

Fig. Simulated phase diagrams of the nanostructure morphologies for substrate temperatures and volume fractions at deposition rates of (a) 300 and (b) 3,000 nm/h.

Ref. Y. Ichino et al., Jpn. J. Appl. Phys. 56 (2017) 015601, IEEE TAS 27 (2017) 7500304

Previous study Monte Carlo simulation for BMO+REBCO crystal growth

BMO self-organization → substrate temperature, volume fraction, depo. rate

BMO nucleation and growth → **surface diffusion**

Objective

Supersaturation and surface diffusion are important
for high-performance REBCO coated conductors.

Estimation of supersaturation and surface diffusion constant via surface morphologies of SmBCO thin films

SmBCO thin films were deposited by pulsed laser deposition (PLD) method.

Detailed observation of surface morphologies of the SmBCO films

Surface diffusion constant → diameter of central 2D-island (top terrace of pancake-like island)

Supersaturation → terrace width

Outline

1. Introduction

(1) Favorable orientation of $REBa_2Cu_3O_y$ films

(2) Self-organization of Ba-M-O (BMO, M=Zr, Sn, Hf, Nb etc.)

Objective

2. Experimental

3. Results and discussion

(1) Surface diffusion constant

(2) Supersaturation and preferential orientation

4. Summary

2. Experimental

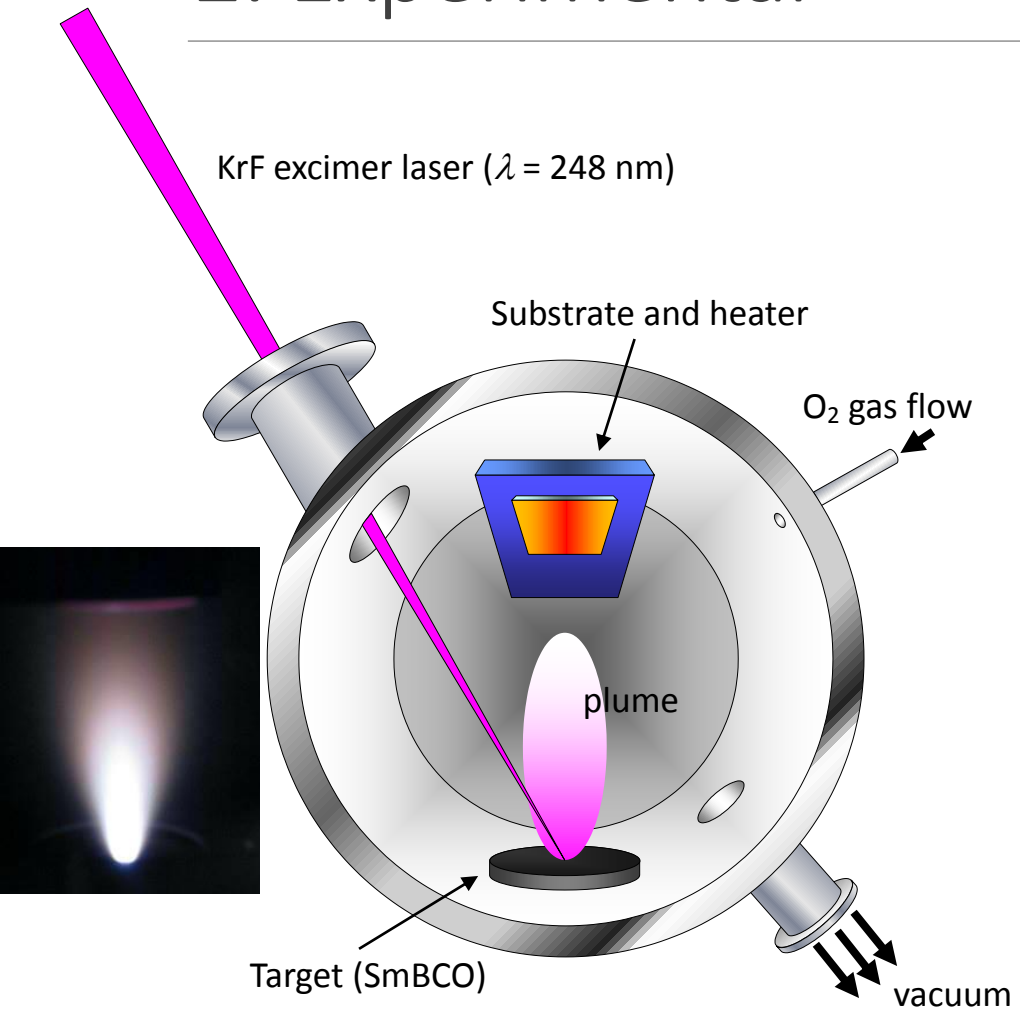

Fig. Schematic drawing of PLD chamber and the photograph is plume of SmBCO.

Table. Deposition conditions

Parameter	Condition
Laser	KrF excimer (λ = 248 nm)
Laser repetition rate, f_L	1 ~ 100 Hz
Laser energy density	1.0 ~ 1.7 J/cm^2
Substrate temp., T_s	760 ~ 880ºC
substrate	$LaAlO_3$ (100) single crystal
target	$SmBa_2Cu_3O_y$ sintered bulk
O_2 pressure	400 mTorr
Clearance between Target and substrate	52.5 mm
Film thickness	Approx. 200 nm

Table. Evaluation method

Evaluation	Method
Orientation	X-ray diffraction (XRD)
Surface morphologies	Atomic force microscopy (AFM)
Composition	Energy Dispersive X-ray spectroscopy (EDX)

Outline

1. Introduction

(1) Favorable orientation of $REBa_2Cu_3O_y$ films

(2) Self-organization of Ba-M-O (BMO, M=Zr, Sn, Hf, Nb etc.)

Objective

2. Experimental

3. Results and discussion

(1) Surface diffusion constant

(2) Supersaturation and preferential orientation

4. Summary

(1) Surface diffusion constant

"In the case of 2D-island and growth, the size Λ_0 of the central 2D-island is a measure for $\pi(D/f_L)^{1/2}$, since new nuclei form only if adatoms are unable to reach the step edge."

[Ref. B. Dam et al., Physica C 305(1998)1]

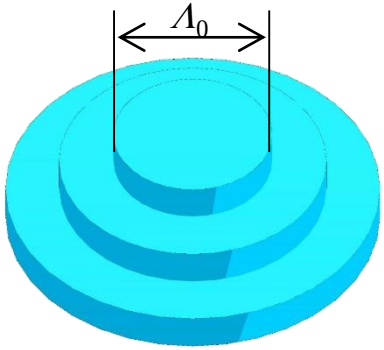

$$\Lambda_0 = \pi\sqrt{D(T_s)/\ f_L}$$

Λ_0 : maximum diameter of the top layer
T_s : substrate temperature
f_L : laser repetition rate
$D(T_s)$: diffusion constant at a T_s

Fig. Estimation of surface diffusion constant from 2D-islands growth.

Surface morphologies of SmBCO thin films deposited at various T_ss and f_Ls

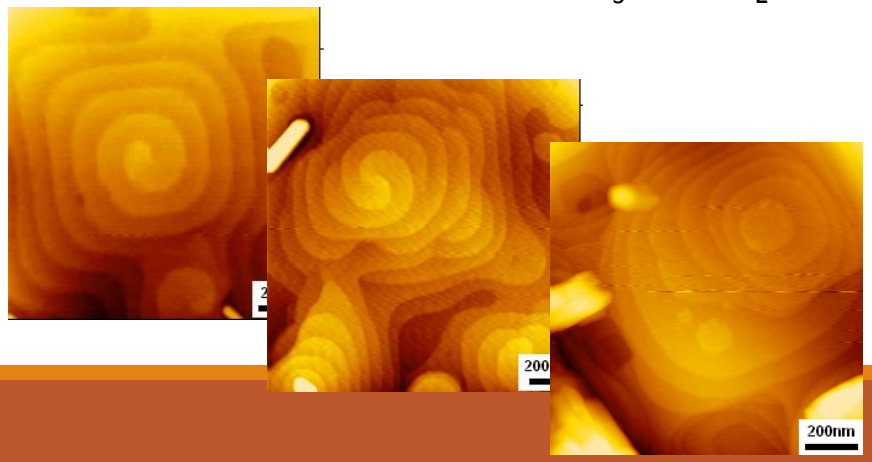

$D(T_s)$ depending on T_s and f_L

Activation energy of Surface diffusion

Surface morphologies of SmBCO thin films

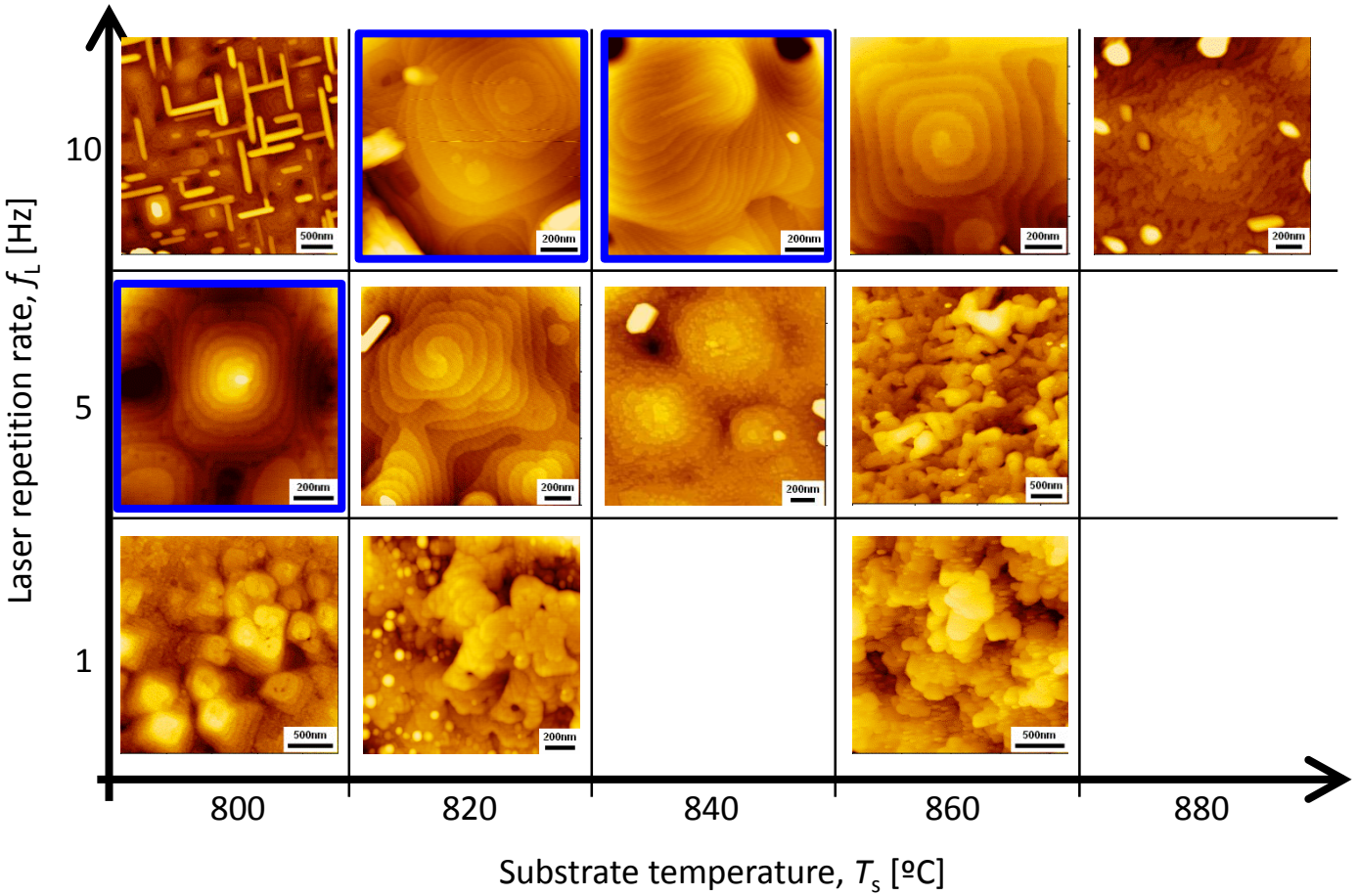

Fig. A part of surface morphologies of SmBCO thin films deposited at T_s = 800~880ºC and f_L =1 ~10 Hz. Morphologies of 2D-island growth are enclosed by blue lines.

$D(T_s)$ are estimated by using $\Lambda_0 = \pi\sqrt{D(T_s)/f_L}$

$D(T_s)$ as a function of T_s

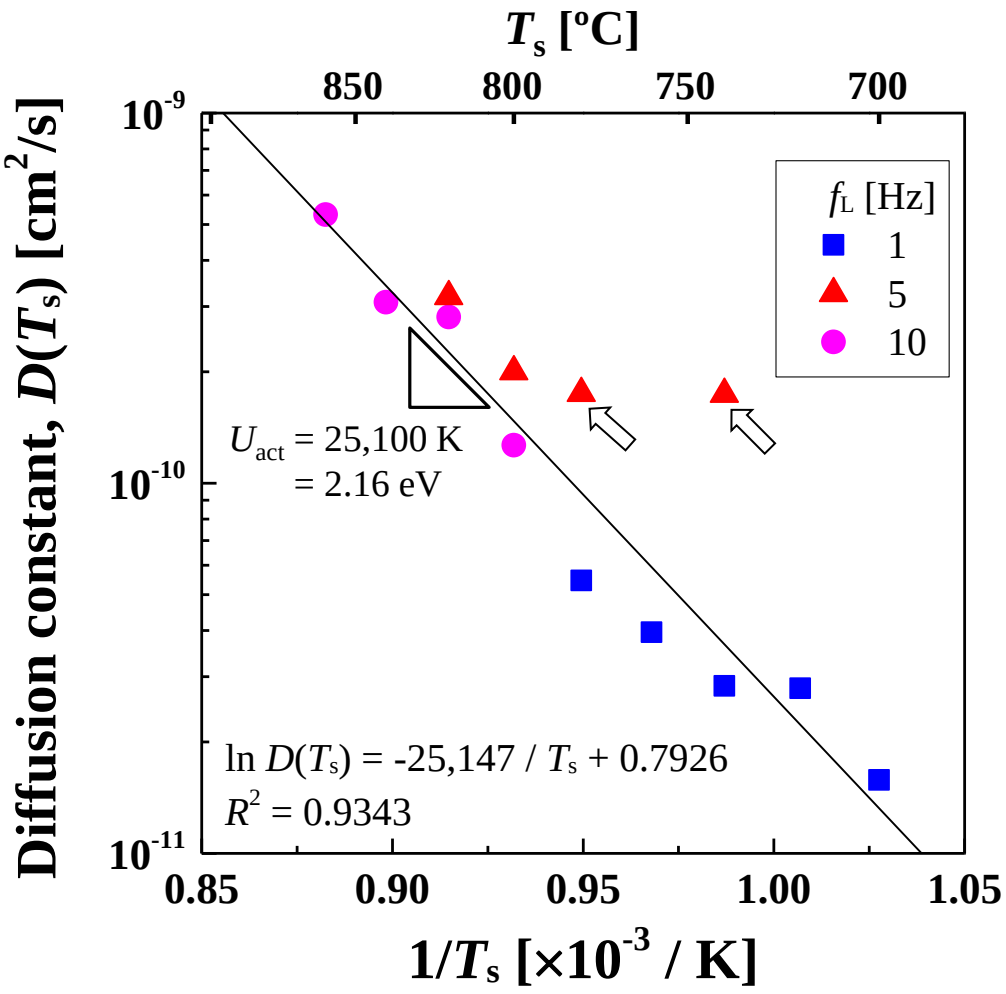

- In spite of f_L, $D(T_s)$ are on the same straight line.
- From the slop of the straight line, activation energy of $D(T_s)$ is estimated.

Activation energy of surface diffusion

U_{act} = 25,100 K = 2.16 eV

Ref. YBCO thin films

U_{act} = 2.5 eV

B. Dam et al., Physica C 305 (1998) 1

Fig. Arrhenius plot of the diffusion constants depending on T_s and f_L. Some data pointed by open arrows are out of trend.

(2) Supersaturation and preferential orientation

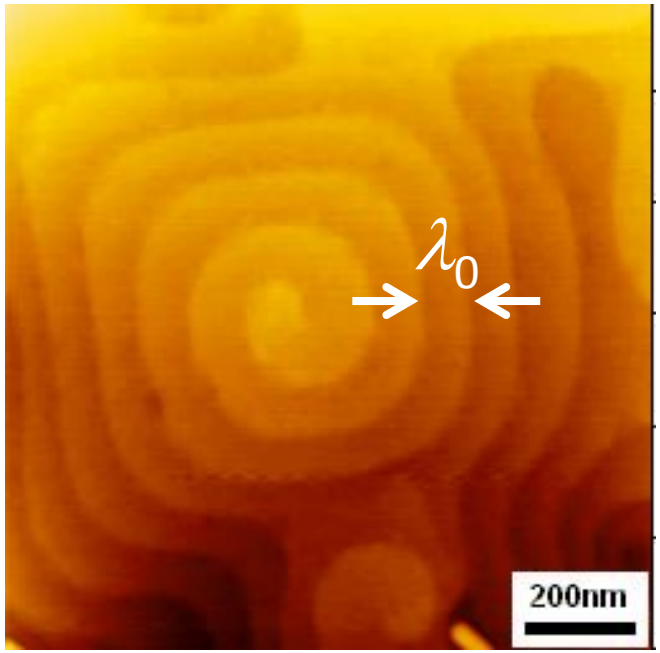

Fig. Surface image of a SmBCO thin film having spiral growth mode.

$$19r^* = \lambda_0$$

$$r^* = \frac{\nu\sigma}{\Delta\mu}$$

r^* : critical radius in nucleation
λ_0 : terrace width of spiral growth
ν : unit cell volume
σ : surface free energy
We used σ = 0.82 J/m^2 for (100) of YBCO.
$\Delta\mu$: supersaturation

Ref. T. Nishinaga et al., Adv. Supercond. 8 (1996) 33

$$\Delta\mu = 19\frac{\nu\sigma}{\lambda_0}$$

Estimation of $\Delta\mu$
From surface morphologies

Surface morphologies of SmBCO thin films deposited at various T_ss and f_Ls

- $\Delta\mu$ depending on T_s and f_L
- Effect of seed layer

Preferential orientation for T_s and f_L

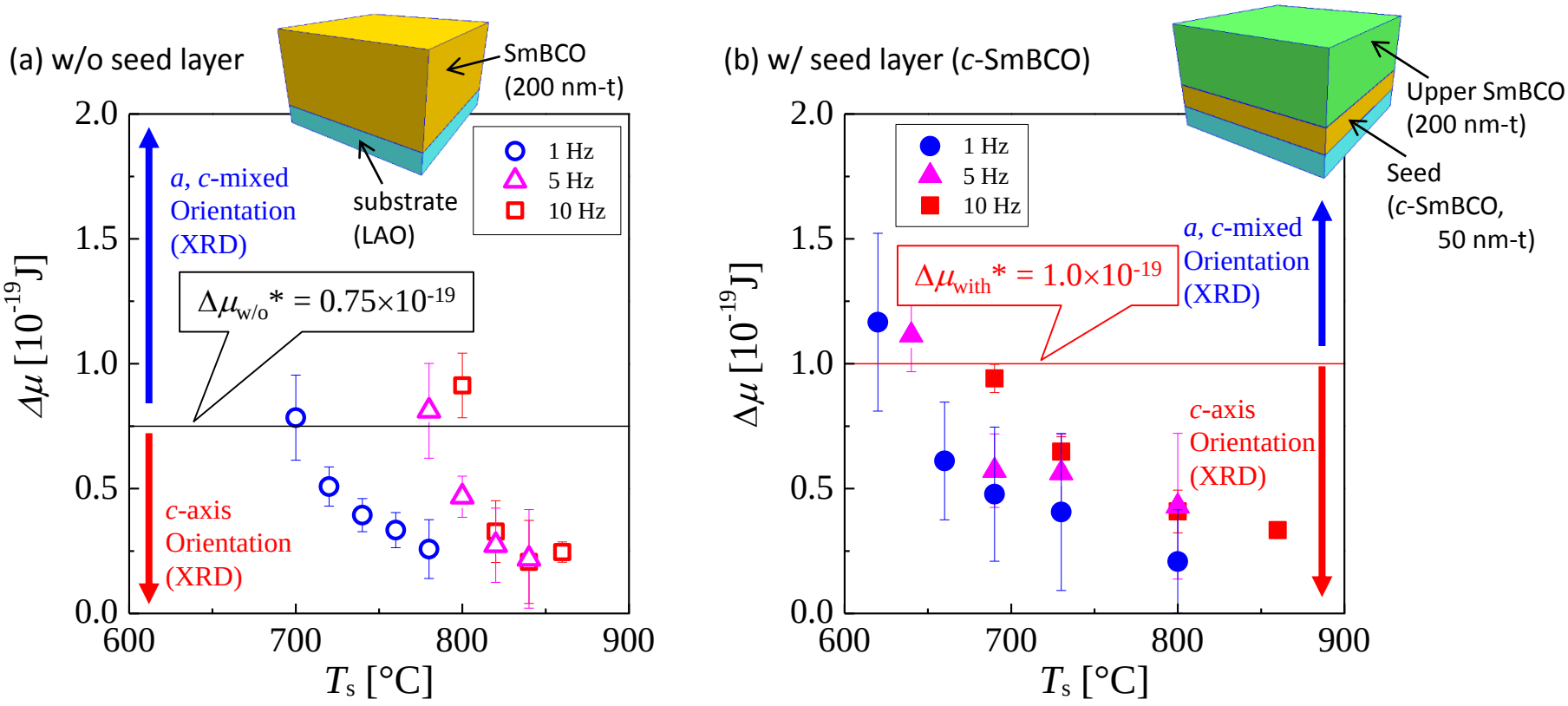

Fig. Substrate temperature (T_s) and laser repetition rate (f_L) dependence of $\Delta\mu$. (a) without seed layers and (b) with seed layers. The seed layers are *c*-axis oriented SmBCO layers deposited at relatively high T_s.

- With increasing T_s and decreasing f_L, $\Delta\mu$ decreased.
- From XRD, *a*-axis oriented grains grew, when $\Delta\mu$ became larger than a threshold $\Delta\mu$ ($\Delta\mu^*$).
- $\Delta\mu^*$ is increased by seed layer (*c*-axis oriented SmBCO) → **Suppression of *a*-axis grain growth**

a-axis and $\Delta\mu$ for high f_L up to 100 Hz

Surface morphologies of SmBCO thin films deposited at T_s = 850ºC and f_L up to 100 Hz

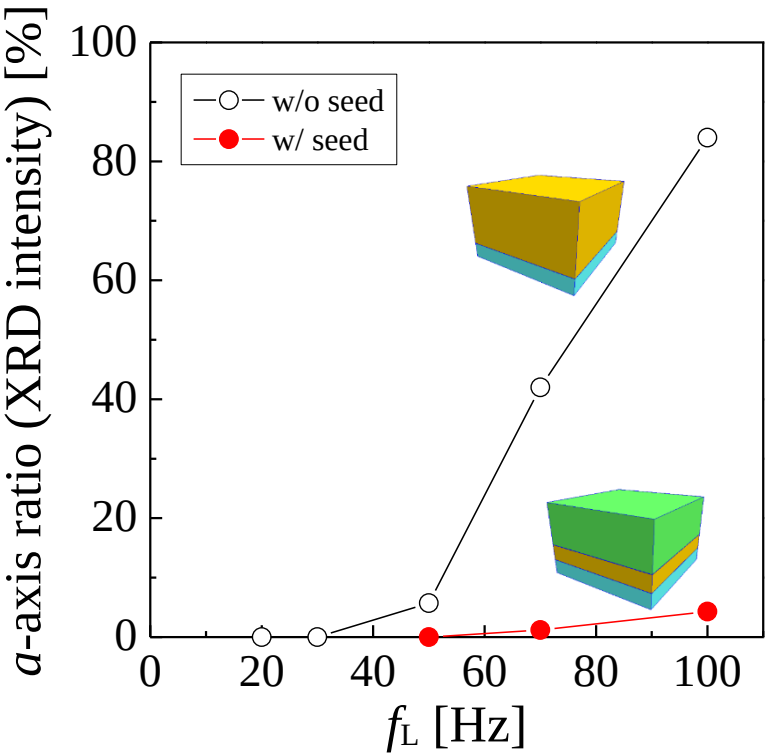

Fig. f_L dependence of *a*-axis ratio, where *a*-axis ratios are estimated from XRD intensity ratio.

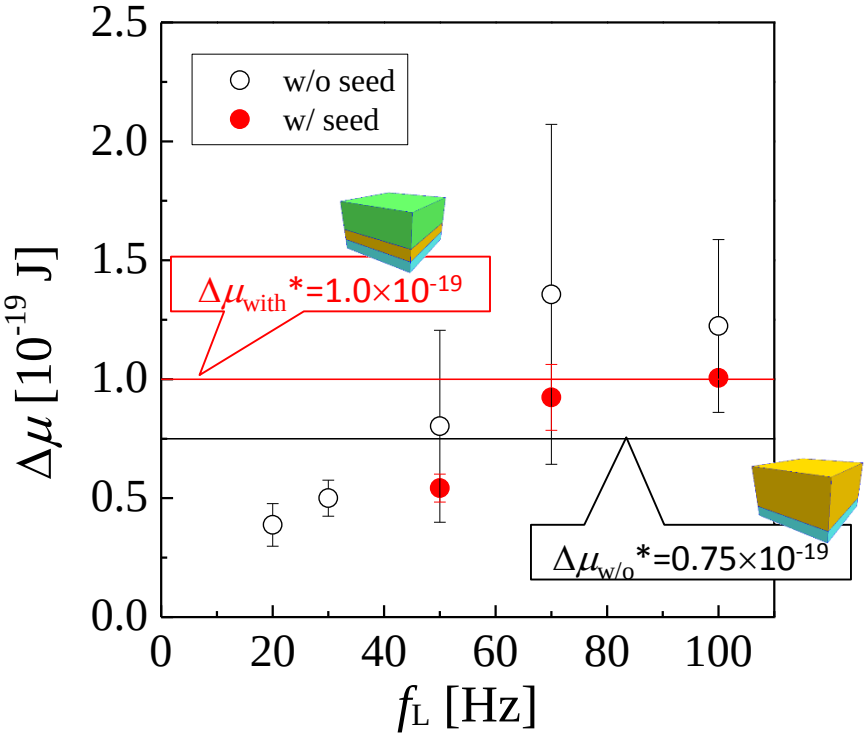

Fig. f_L dependence of $\Delta\mu$, where $\Delta\mu$ are estimated from terrace width of the films. Here, the $\Delta\mu$*s are The values estimated in the previous slide.

- *a*-axis grains increased with increasing f_L. $\Delta\mu$ also increased with increasing f_L.
- *a*-axis oriented grains grew, when $\Delta\mu$ became larger than $\Delta\mu$*.

  → Seed layer can suppress *a*-axis grain growth even at high f_L due to the high $\Delta\mu$*.

4. Summary

We estimated surface diffusion constants and supersaturation of SmBCO thin films via the surface morphologies.

➢ Surface diffusion constant

- Surface morphologies are affected by deposition conditions such as T_s and f_L.
- From 2D-island growth mode, $D(T_s)$ are estimated.
- In spite of f_L, there are $D(T_s)$ in the same straight line in Arrhenius plot of $D(T_s)$.
- Activation energy of surface diffusion is estimated and the value is **2.2 eV**.

➢ Supersaturation and preferential orientation

- $\Delta\mu$ are also estimated from surface morphologies of SmBCO thin films.
- *a*-axis oriented grains grew, when $\Delta\mu$ became larger than threshold $\Delta\mu$ ($\Delta\mu^*$).
- With increasing T_s and decreasing f_L, $\Delta\mu$ decreased.
- $\Delta\mu^*$ is increased by seed layer (*c*-axis oriented SmBCO)

→ **Suppression of *a*-axis grain growth**

Quasi Homo-Epitaxial Nucleation (QHEN) model

ref. Y. Ichino et al., IEEE TAS 13 (2003) 2735

σ : surface energy
v : unit cell volume

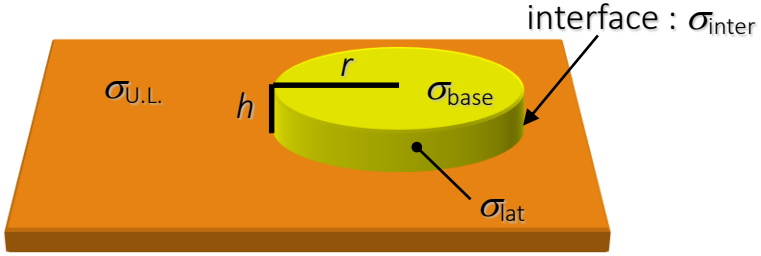

Nucleation on *c*-axis oriented underlying layer

Critical nucleation energy

$$\Delta G^* = \frac{\pi (h\sigma_{lat})^2}{(h/v)(\Delta\mu - \Delta\mu^*)}$$

Critical supersaturation of nucleation

$$\Delta\mu^* = \frac{v}{h}(\sigma_{base} + \sigma_{inter} - \sigma_{U.L.})$$

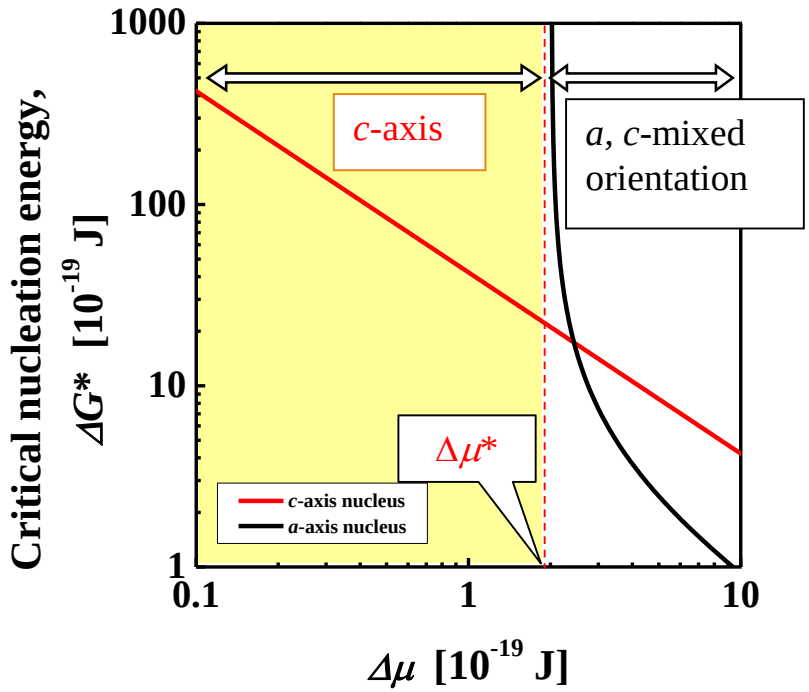

Fig. Critical nucleation energy of REBCO as a function of supersaturation.

Table Surface free energy densities of YBCO for different orientation of nuclei and estimated critical supersaturation of nucleation.

Orientation of nuclei	σ_{base}[J/m^2]	σ_{lat}[J/m^2]	σ_{inter}[J/m^2]	$\sigma_{U.L.}$[J/m^2]	$\Delta\mu^*$ [J]
c-axis	0.59(=$\sigma_{(001)}$)	0.82(=$\sigma_{(100)}$)	0	0.59	0
a-axis	0.82(=$\sigma_{(100)}$)	0.59(=$\sigma_{(001)}$)	0.23 (=$\sigma_{(100)}$-$\sigma_{(001)}$)	0.59	2.1×10^{-19}

c-axis orientation is encouraged at lower $\Delta\mu$.
(high T_s, low deposition rate)

a-axis grain growth with thickness

Ref. T. Watanabe et al, IEEE TAS 15 (2005) 2620

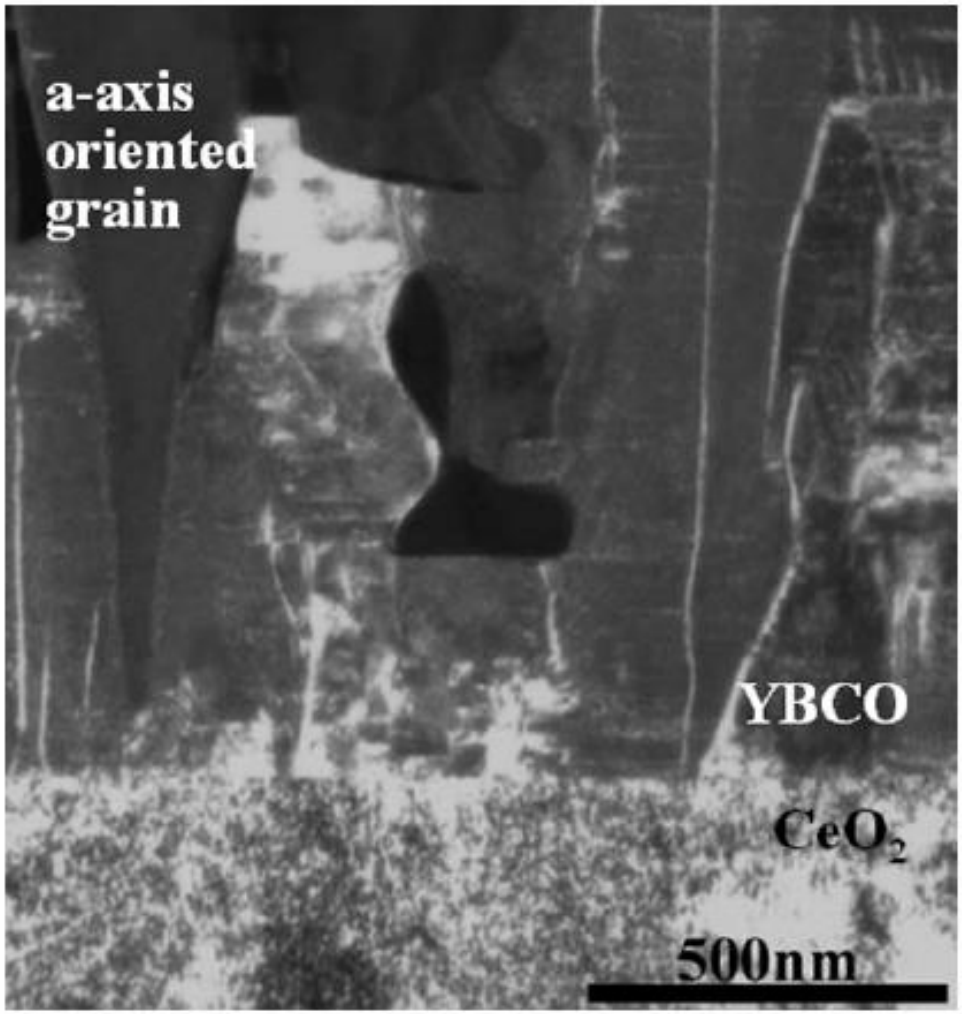

An *a*-axis grain nucleates on the CeO_2 surface.

The *a*-axis grain enlarged with increasing film thickness.

Fig. 4. Cross-sectional TEM dark-field electron micrograph of the YBCO film on PLD-CeO_2 using the $\langle 206 \rangle$ of YBCO reflections.

Nanorods morphology (Experimental)

BHO-dope SmBCO films by PLD method

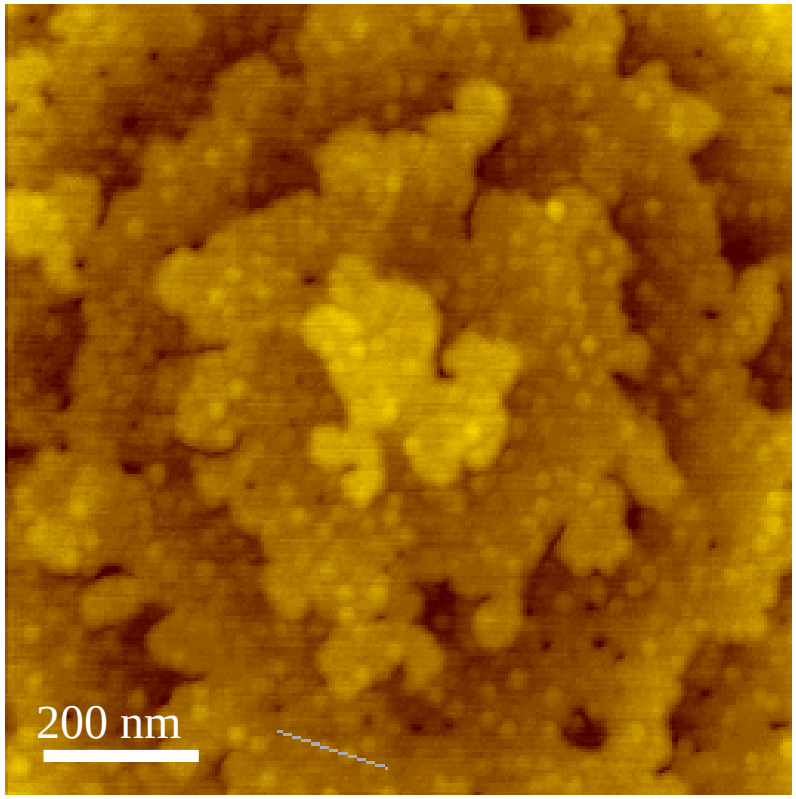

Fig. DFM images for 3.0 vol.% BHO-doped SmBCO films deposited at T_s = 870ºC (1,143 K).

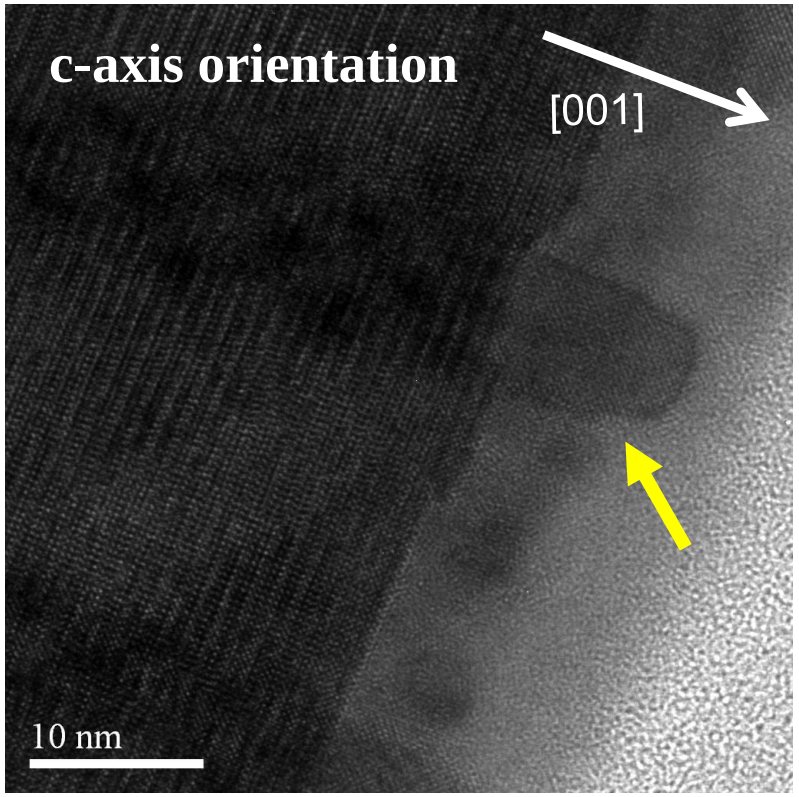

Fig. Cross-sectional TEM image around film surface of 3.0 vol.% BHO-doped SmBCO film.

(left figure) Many particle-like nano-structures.
(right figure) Nanorod threw out from REBCO.

Consistent with 3D-MC Simulation results

Growth temperature dependence of number density

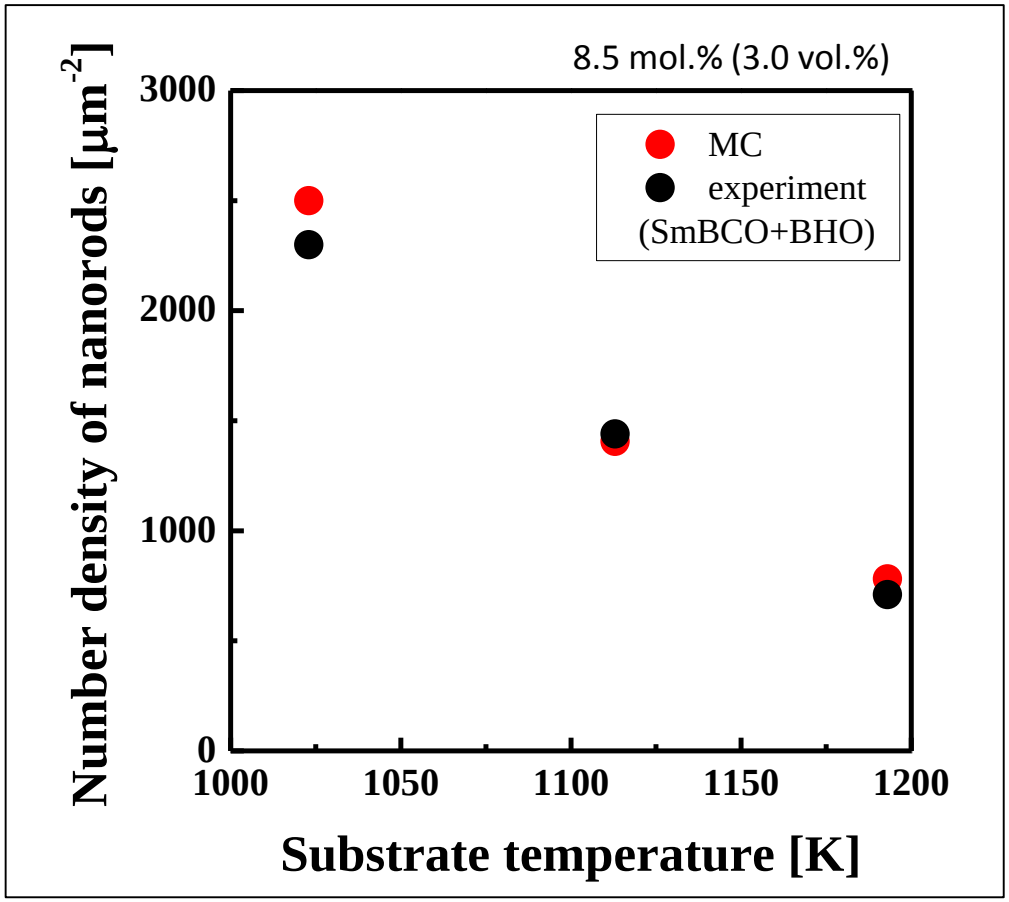

- The T_s dependence of the number density was reproduced well.
- The simulation parameters which can reproduce our experimental results are chosen.

We can reproduce
the self-organization
by the 3D-MC simulation.

Simulation model (two-components system)

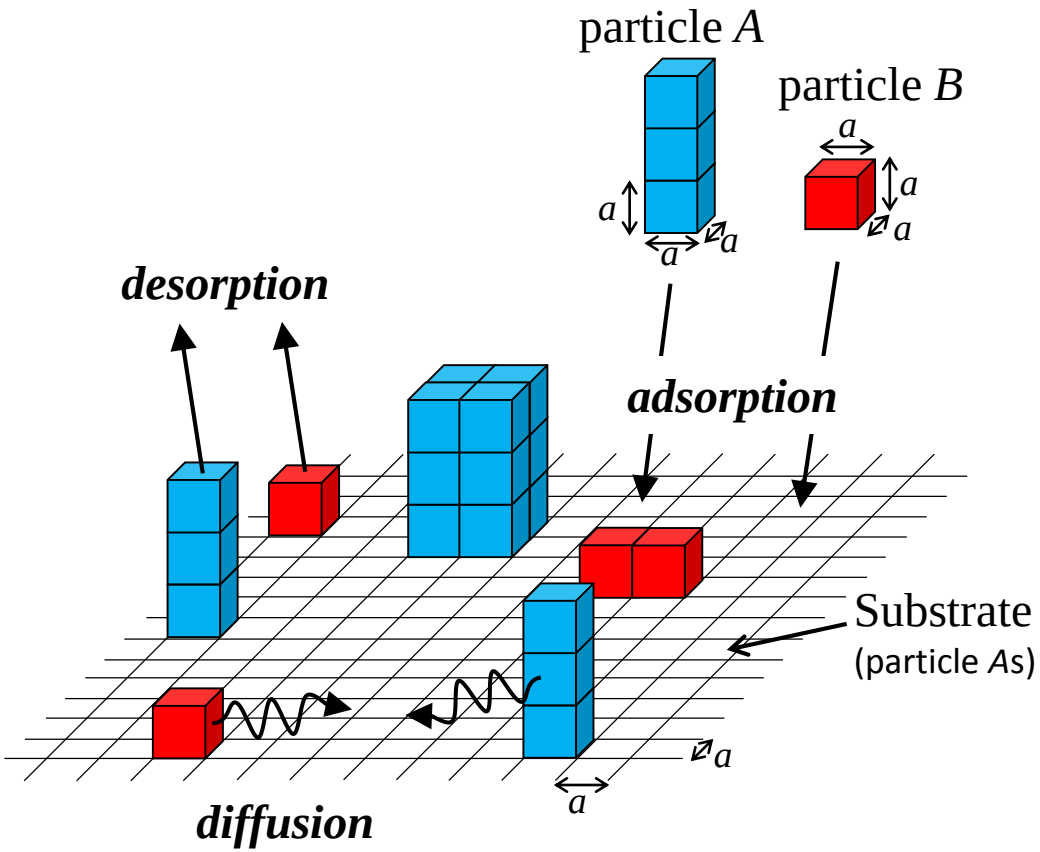

Fig. Schematic illustration of MC events in our simulation. Two types of particles are used in this model. Substrate is consisted of particle As.

➢ Energy state of the particles

- Isotropic bond energy density
- Counting bonds between the nearest neighbors

$\Delta E = E_f - E_i$ E_i : initial state, E_f : final state

➢ Particle motions

- Two types of particles are deposited onto the substrate.
- One of adsorption and diffusion motions is randomly chosen by a probability of *R*.

$$R = \frac{(\#\text{ of adsorp. in unit time})}{(\#\text{ of diffu. in unit time})} = \frac{Fa^2}{D/a^2} = \frac{Fa^4}{D}$$

F: incident flux [/m^{2}s]
D: diffu. const. [m^2/s]

- Moving only to a nearest neighbor site.
- A desorption of a particle occurs a probability of $\exp(-E_{des}/k_BT)$.
- Periodic boundary conditions (*x* , *y* directions)

Energy state (bond energies)

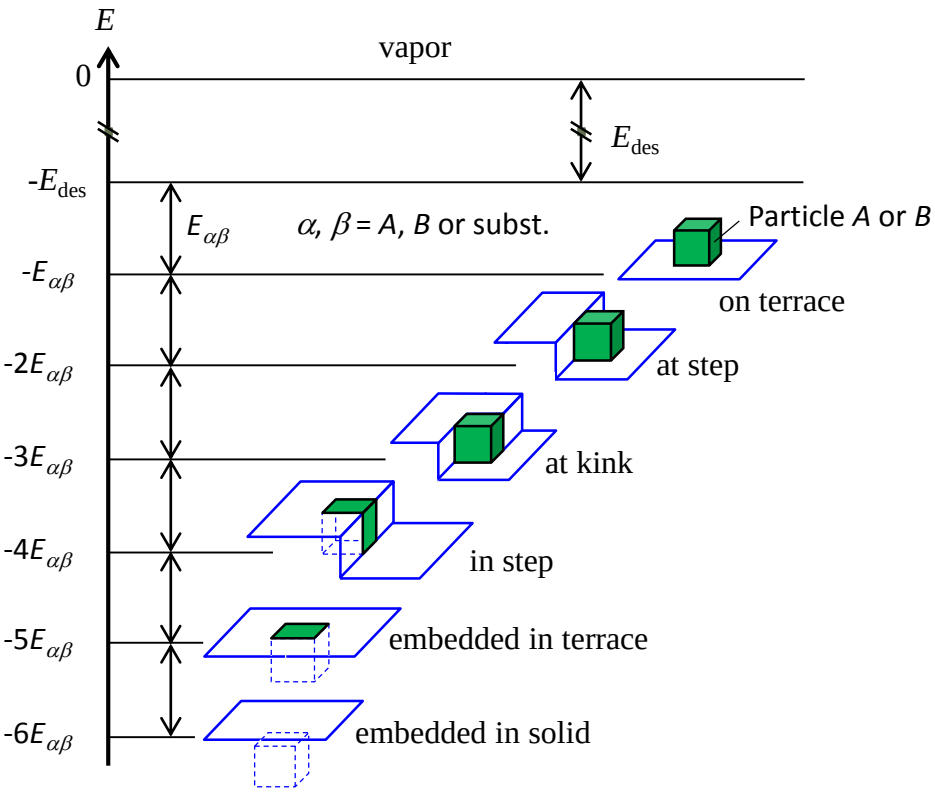

Fig. Energy state diagram of the adsorbed particles on the substrate.

Table Bonding **energy densities per a^2.**

E_{AA} (A-A)	2,000 K
E_{BB} (B-B)	2,500 K
E_{AB} (A-B)	500 K
E_{AS} (A-subst.)	E_{AA}
E_{BS} (B-subst.)	E_{AB}
E_{des}	50,000 K

Table Simulation conditions

Diffusion const., D	~10^{-13} - 10^{-11} cm^2/s *
a	0.4 nm
Molar fraction of B	8.5 mol.% (3 vol.%)
Depo. rate, v_{dep}	10 ~ 3,000 nm/h

* B. Dam et al., Physica C 305 (1998) 1

- The initial and final states are calculated based on the bond-counting model.

Deposition rate in this simulation

Number of adsorbed particles on one site of substrate in unit time

Adsorption frequency : $r_{ads} = Fa^2 = \frac{v_{dep}}{3a^3} \cdot a^2$

Number of diffusing particles from one site of substrate in unit time

Diffusion frequency : $r_{diff} = \frac{D}{a^2}$

a : lattice constant [m]
F : incident flux [$m^{-2}s^{-1}$]
v_{dep} : deposition rate [m/s]
D : surface diffusion constant [m^2/s]

Probability of adsorption to surface diffusion at a site on the substrate

Growth kinetic factor : $R = \frac{r_{ads}}{r_{diff}} = \frac{Fa^4}{D} = \frac{v_{dep}a}{3D}$

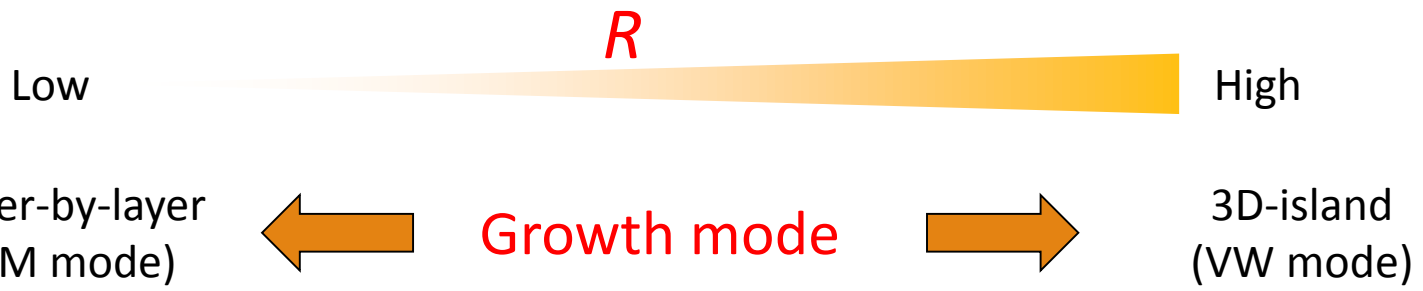

→ We changed the deposition rate by changing the R.

Deposition rate dependence

T_s = 1,193 K (920ºC)

REBCO particles are transparent in these movies.

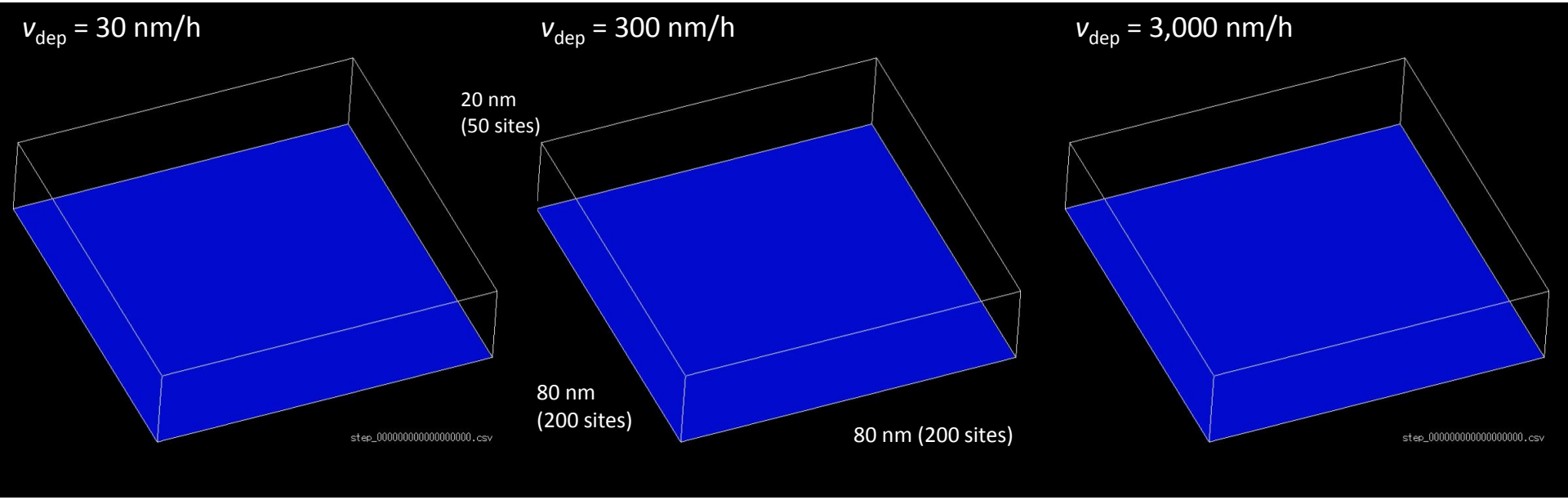

Fig. Deposition rate dependence of nanorods growth at T_s = 1,193 K.

Table. Specifications of the nanorods under each condition.

Deposition rate [nm/h]	Number density [μm^{-2}]	Nanorods morphology
30	625	Straight
300	2,031	Straight
3,000	7,031	inclined

Deposition rate dependence

T_s = 1,023 K (750ºC)

REBCO particles are transparent in these movies.

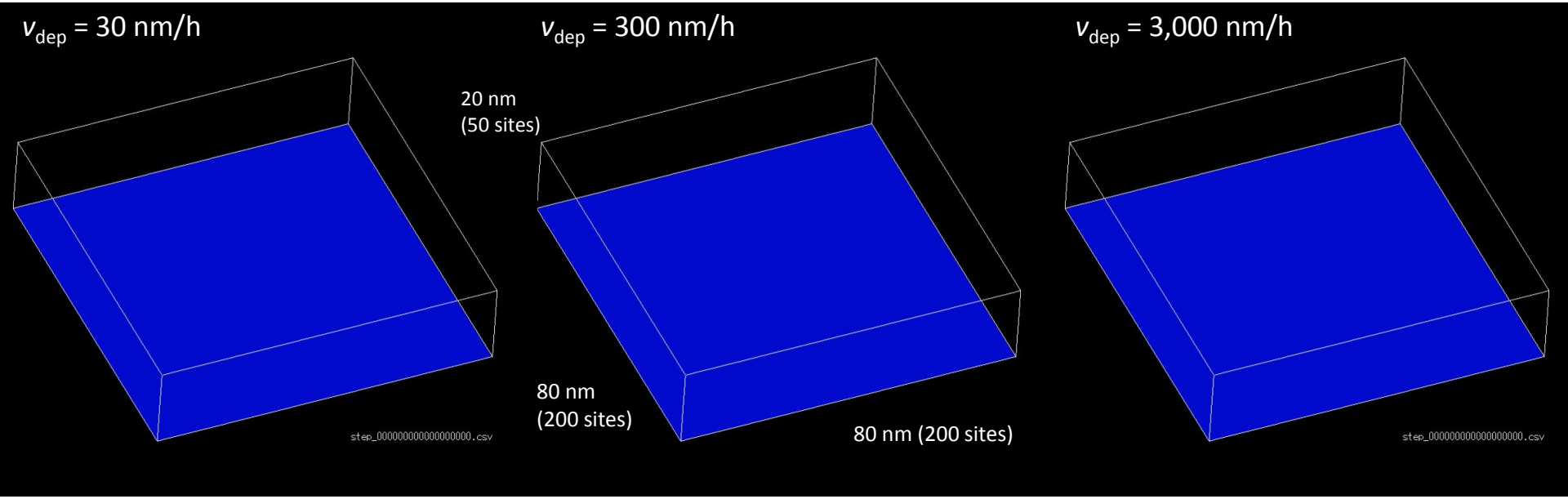

Fig. Deposition rate dependence of nanorods growth at T_s = 1,023 K.

Table. Specifications of the nanorods under each condition.

Deposition rate [nm/h]	Number density [μm^{-2}]	Nanorods morphology
30	2,188	Straight
300	4,531	inclined
3,000	--	Particle

Comparison of growth (T_s = 1,023 K)

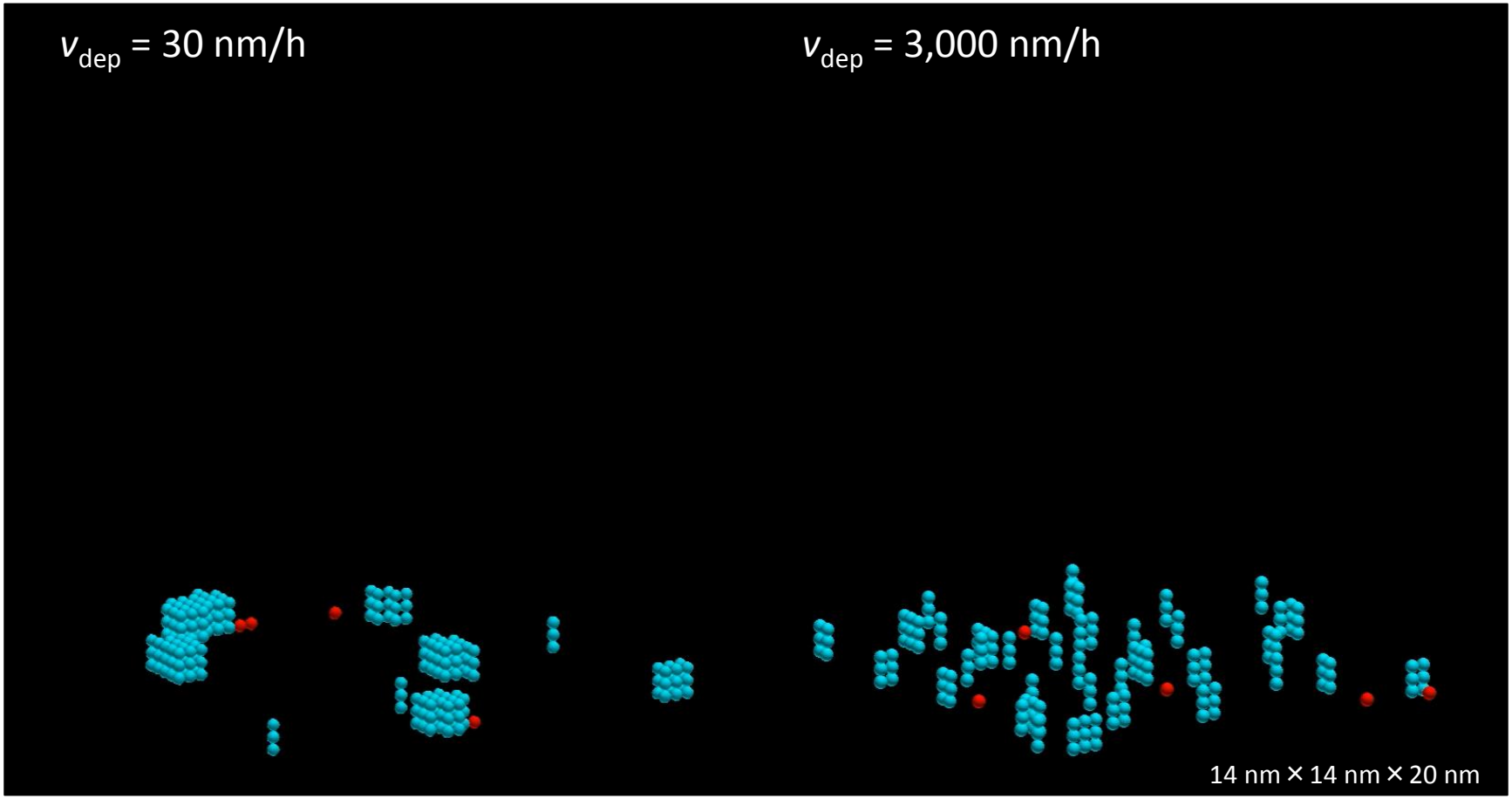

- v_{dep} = 30 nm/h: BMOs were able to aggregate into one 3D-island due to low advanced speed of REBCO growth front.
- v_{dep} = 3,000 nm/h: There were many small BMO clusters. The BMO clusters were capped by the REBCO due to the high advanced speed of the REBCO growth front.
- Higher deposition rate leads to insufficient nanorods growth.

Growth temperature dependence

- v_{dep} = 100 nm/h, m_{BMO} = 8.5 mol.% (3 vol.%)
- Particle *A*s are transparent in these movies.

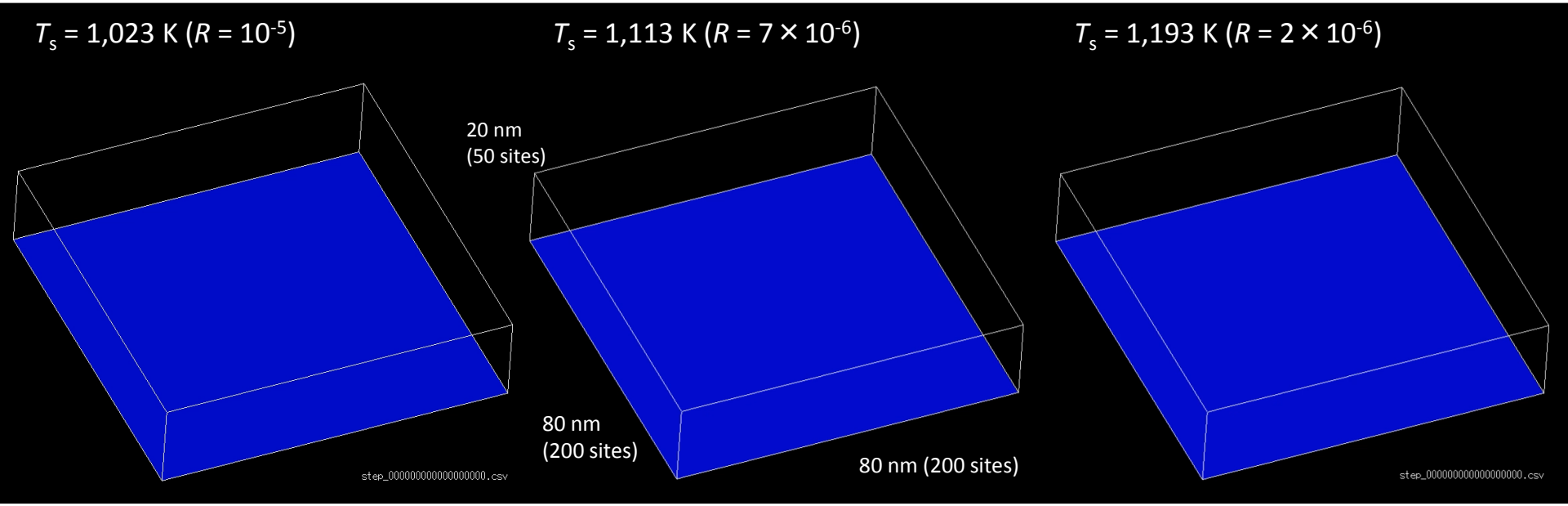

Fig. Time dependents of nanorods-growth in different substrate temperatures.

- Particle *B*s grew up into nanorod shape within particle *A*s.
- The number density of the nanorods decreased with increasing T_s.
- At T_s = 1,023 K, there were tilting nanorods.

Phase diagram of surface morphologies

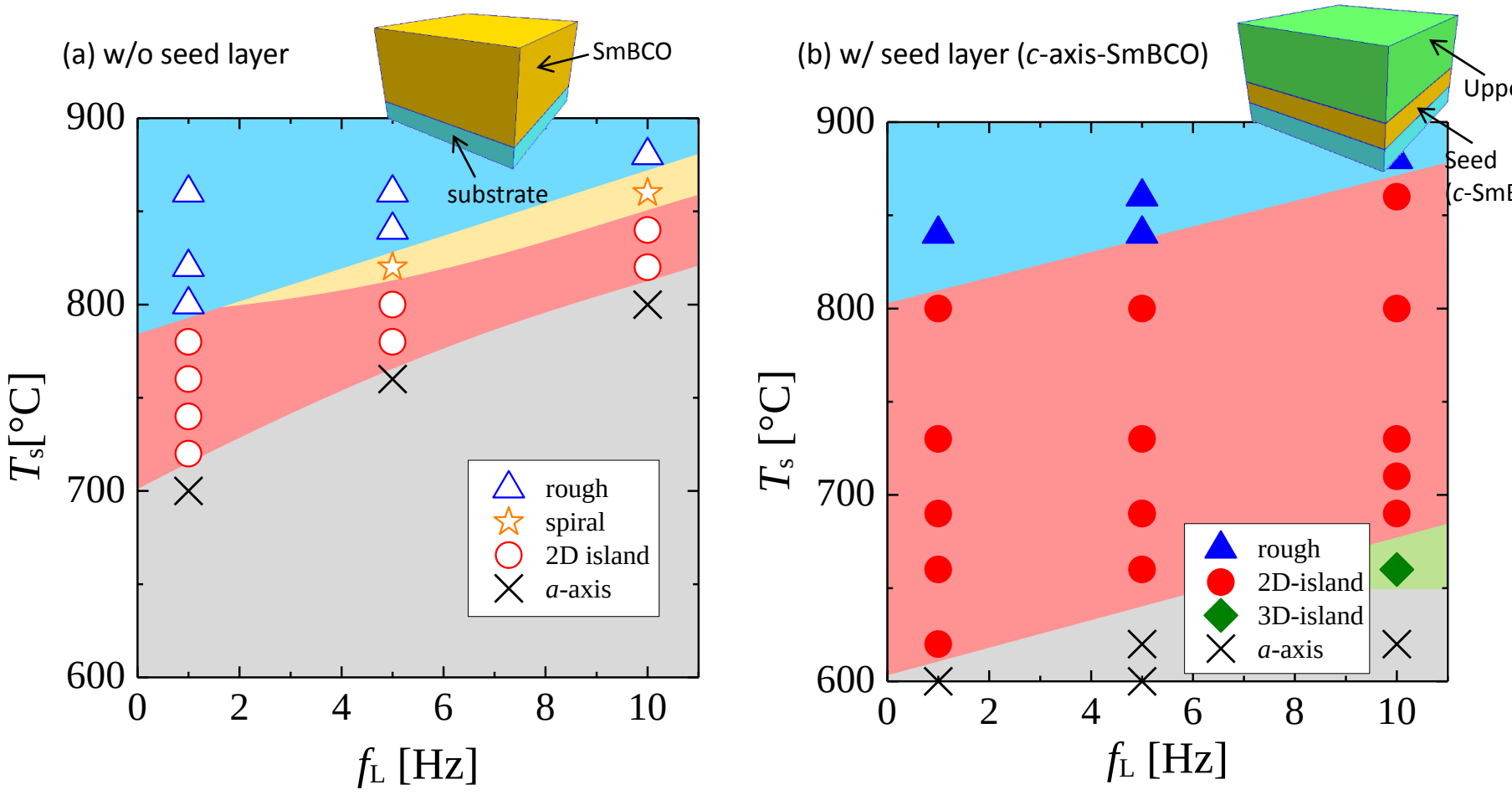

Fig. Phase diagrams of surface morphologies of SmBCO films depending on substrate temperature (T_s) and laser repetition rate (f_L) (a) without seed layers and (b) with seed layers.
The seed layers are *c*-axis oriented SmBCO layers deposited at relatively high T_s.